

## Metal recognition behaviour study of coumarin containing benzimidazole moiety

Keerthika Kumarasamy<sup>1</sup>, Tamiloli Devendhiran<sup>2</sup>, Wei-Jyun Chien<sup>1</sup>, Mei-Ching Lin<sup>1</sup>, Selva Kumar Ramasamy<sup>3</sup>, Chih-Jung Chen<sup>1</sup>, Jui-Chang Tseng<sup>1\*</sup>

<sup>1</sup>Department of Applied Chemistry, Chaoyang University of Technology, Taichung, 413310, Taiwan (R.O.C)

<sup>2</sup>Department of Chemistry, National Changhua University of Education, Changhua, 500, Taiwan (R.O.C)

<sup>3</sup>Department of Chemistry, Maharishi Markandeshwar Engineering College, Maharishi Markandeshwar (Deemed to be) University, Ambala, 133207, Haryana, India

### ABSTRACT

A series of chemical-sensors, benzimidazole-coumarin (M1, M2 & M3), were synthesized and characterized by <sup>1</sup>H NMR, mass spectrometry, and elementary analysis. UV-Vis absorption and emission spectrometer investigated the fluorescent behavior and recognition mechanism of these sensors. The absorption and emission bands of sensor M derivatives were found at 310 to 350 and 390 to 580 nm. The sensor M derivative exhibits a “turn-off” fluorescent quenching and selective complexing capacity towards Cu<sup>2+</sup> ions. The detection limit of sensor M1 is 3.9 nM for Cu<sup>2+</sup> ions, and the coordination ratio was found to be 2:1 ratio by the Job’s plot method. The binding constant was also calculated to be  $K_s 3.41 \times 10^9 / M^2$ . The fluorescence quenching seen in M-Cu<sup>2+</sup> has been attributed to a lower HOMO-LUMO orbital gap and decreased electron donation from the coordinated imidazolyl coumarin, as found by DFT calculations. The sensor M2 was successfully applied to detect Cu<sup>2+</sup> in the different water samples. A stable complex of sensor M-Cu<sup>2+</sup> was characterized by the Job’s plot method, ESI-MS and DFT studies.

**Keywords:** Metal ion sensor, Benzimidazole, Cu<sup>2+</sup> sensing, Coumarin, DFT calculations, EDTA.

### OPEN ACCESS

Received: July 14, 2023


Revised: September 5, 2023

Accepted: October 20, 2023

#### Corresponding Author:

Jui-Chang Tseng

[jetseng@cyut.edu.tw](mailto:jetseng@cyut.edu.tw)

 **Copyright:** The Author(s). This is an open access article distributed under the terms of the [Creative Commons Attribution License \(CC BY 4.0\)](https://creativecommons.org/licenses/by/4.0/), which permits unrestricted distribution provided the original author and source are cited.

#### Publisher:

[Chaoyang University of Technology](https://www.cyut.edu.tw/)

ISSN: 1727-2394 (Print)

ISSN: 1727-7841 (Online)

### 1. INTRODUCTION

Developing a sensitive chemosensor for detecting heavy and transition metal ions in environmental and biological fields has attracted much interest in recent years (Gunnlaugsson et al., 2006; Kim et al., 2008). The design and synthesis of molecules with specific areas for binding and signaling components, which can exhibit distinct changes in their fluorescence when a target molecule binds to them, have always been critical in molecular fluorescent sensor detection (Waggoner et al., 1999; Valentine et al., 2003; Sathiyam et al., 2016). Selective sensor protocols are essential for heavy and transition metal ions, particularly paramagnetic Cu<sup>2+</sup>, a vital trace element that acts as a cofactor in various critical biological processes across all living organisms (Strausak et al., 2001; Sathiyam et al., 2016). Still, changes in its cellular homeostasis have been linked to severe neurodegenerative disorders (Mercer et al., 2001). According to the World Health Organization (WHO) and the European Union-Water Framework Directive (EU-WFD), the maximum allowable quantity of copper ions in drinking water samples is 2 mg/L (Saleem et al., 2018; Liu et al., 2019). Due to its essential yet toxic nature, cells strictly manage internal copper distributions, and free copper ions in the cytoplasm are considerably below one per cell using thermodynamic calculations (Rae et al., 1999;

Puig et al., 2002., Sathiyam et al., 2019). Therefore, very sensitive optical imaging using a copper-selective luminescent detector is required to visualize kinetically labile copper at the molecular level (Yu et al., 2008; Jung et al., 2009; Sathiyam et al., 2019). The divalent copper ion is an excellent, efficient fluorescence quencher in many fluorophores by various mechanisms, including energy transfer, electron transfer, and static quenching, but the fluorescent enhancement for  $\text{Cu}^{2+}$  binding is relatively weak, presenting a substantial design difficulty (Haugland, 2002; Kim et al., 2006). Several factors can interfere with measurement accuracy beyond the apparent shift in fluorescence intensity due to metal binding. These include instrumental efficiency, environmental conditions, including temperature and pH, and the concentration of the fluorescent probe.

In recent years, fluorescence chemosensors have gained significant attention for detecting  $\text{Cu}^{2+}$  ions due to their advantages over traditional analytical methods in terms of sensitivity, selectivity, simplicity, and non-destructiveness (Sahoo et al., 2016; Venkatesan et al., 2019). Copper ions may be monitored using several diverse mediums, including rhodamine, coumarin, fluorescein, BODIPY and cyanine (Huang et al., 2021; Kumarasamy et al., 2022). The fluorescence sensors based on coumarin derivatives described in the literature are among the most sensitive and selective of these organic compounds for detecting  $\text{Cu}^{2+}$  ions with high accuracy (Devendhiran et al., 2021). There has been some research on using coumarin derivative-based fluorescent chemosensors for  $\text{Cu}^{2+}$  monitoring in aqueous samples. Our study includes the development of novel sensors for the selective detection of specific metal ions. Our lab has described a novel indole and BODIPY-based chemosensor for  $\text{Cu}^{2+}$  and  $\text{Ni}^{2+}$  ions (Huang et al., 2021; Kumarasamy et al., 2022) and a coumarin-based chemosensor for  $\text{CN}^-$  ions (Devendhiran et al., 2021). However, the number of studies is relatively limited. A coumarin and benzimidazole-based pyridine fluorescent sensor have been developed for detecting  $\text{Cu}^{2+}$  ions in deionized water, and the detection limit was 8.5 and 3 nM (Kumarasamy et al., 2022; Kumarasamy et al., 2023). Moreover, the detection limits in the above-mentioned studies are still lower than the legal acceptability values given by WHO and EU-WFD standards for drinking water samples (31.5  $\mu\text{M}$ ). Consequently, coumarin-based fluorescent chemosensors for  $\text{Cu}^{2+}$  ions with high accuracy and recovery values are in great demand.

To address the issues mentioned above, a new series of coumarin-based molecular systems for the sensitive and selective detection of  $\text{Cu}^{2+}$  ions has been developed. Coumarin can be used as a chromophore due to its excellent photophysical properties, including high quantum yield, good photostability, large Stokes shift, and moderately high water solubility (Yuan et al., 2011; Feng et al., 2019; Sathiyam et al., 2021). Here, we design and synthesize a series of coumarin-based chemosensor M derivatives, which can detect  $\text{Cu}^{2+}$  ions in an aqueous medium. The

structure of the sensing molecule combines two fluorescent groups, benzimidazole and coumarin, as the structure's skeleton. The -OH functional group of the coumarin and the imine on benzimidazole are modified to provide a coordination position to sense metal. In addition, a push-pull electron group was introduced on the benzimidazole unit to explore the influence of changes in photochemical properties and metal ion recognition.

## 2. EXPERIMENTAL

### 2.1. Materials and Methods

Sensor M was prepared using the standard procedure as described in the literature (Devendhiran et al., 2021). All synthesis chemicals were obtained commercially, and the solvents were of analytical grade. Perchlorate salts were purchased from Alfa-Aesar Chemical Reagent Co, Taiwan, and used as received.

FTIR spectra were recorded using a Perkin Elmer Spectrum Two FT-IR spectrometer in ATR mode. Melting points were determined using an MP-ID. The absorption spectra were recorded using a Perkin Elmer PDA UV/Vis Lambda 265 spectrometer. The photoluminescence spectra were recorded on a JASCO FP-8500 spectrofluorimeter by using a 5 nm slit at room temperature.  $^1\text{H}$  NMR spectra were recorded on a VARIAN 200 MHz spectrometer using  $\text{CDCl}_3$  and  $\text{DMSO-}d_6$  solvent. Mass spectra were obtained using a SHIMADZU GC-2010 plus and Finnigan/Thermo Quest MAT 95XL mass spectrometer. The microanalysis of carbon, hydrogen, and nitrogen was determined using a Vario EL III CHN elemental analyzer for evaluating analytical function.

### 2.2. Preparation of Benzimidazole-Coumarin Ligands

The ligands were prepared using a general procedure in which 1, 2-substituted diaminobenzene (0.25 mmol) with 7-hydroxy-4-methyl-2-oxo-2H-chromone-8-carbaldehyde (L) (0.25 mmol) in the presence of ammonium acetate (2.50 mmol) in ethanol 10 mL. The resulting solution was refluxed for 18 h, and the reaction progress was monitored by TLC. After completing the conversion, the solution was cooled and poured into 50 mL of ice water to produce a precipitate, which was filtered by suction, washed with water, and dried. Finally, column techniques purified the crude with ethyl acetate/hexane (3:7) as the eluent to get compounds (M).

#### 2.2.1. Sensor M1

Color: Yellow solid; Yield: 97%; Melting point: 273–275°C;  $^1\text{H}$  NMR (200 MHz,  $\text{CDCl}_3$ )  $\delta$  7.74-7.69 (m, 2H), 7.61-7.56 (d, 1H,  $J = 8.8$  Hz), 7.38-7.34 (m, 2H), 7.11-7.07 (d, 1H,  $J = 8.6$  Hz), 6.18 (s, 1H), 2.47 (s, 3H) ppm; MS (EI)  $m/z = 293.21$  (M + H) $^+$ ; Elemental analysis ( $\text{C}_{17}\text{H}_{12}\text{N}_2\text{O}_3$ ); Theoretical: C, 69.8567; H, 4.4382; N, 9.5841 (%); Actual: C, 68.92; H, 4.72; N, 8.66 (%).

### 2.2.2. Sensor M2

Color: Yellow solid; Yield: 63%; Melting point: 248–250°C;  $^1\text{H NMR}$  (200 MHz,  $\text{CDCl}_3$ )  $\delta$  11.09 (br, 1H), 7.65–7.43 (m, 3H), 7.19–7.15 (d, 1H,  $J = 8.2$  Hz), 7.09–7.04 (d, 1H,  $J = 9$  Hz), 6.16 (s, 1H), 2.52 (s, 3H), 2.46 (s, 3H) ppm; MS (EI)  $m/z = 306.16$  ( $\text{M}^+$ ); Elemental analysis ( $\text{C}_{18}\text{H}_{14}\text{N}_2\text{O}_3$ ); Theoretical: C, 70.5789; H, 4.6069; N, 9.1453 (%); Actual: C, 69.92; H, 4.92; N, 8.49 (%).

### 2.2.3. Sensor M3

Color: Yellow solid; Yield: 81%; Melting point: 308–310°C;  $^1\text{H NMR}$  (200 MHz,  $\text{DMSO}-d_6$ )  $\delta$  8.68 (s, 1H), 8.25–8.20 (d, 1H,  $J = 8.8$  Hz), 7.98–7.93 (d, 1H,  $J = 9.2$  Hz), 7.89–7.84 (d, 1H,  $J = 8.8$  Hz), 7.14–7.09 (d, 1H,  $J = 9$  Hz), 6.31 (s, 1H), 2.43 (s, 3H) ppm; MS (EI)  $m/z = 337.09$  ( $\text{M}^+$ ); Elemental analysis ( $\text{C}_{17}\text{H}_{11}\text{N}_3\text{O}_5$ ); Theoretical: C, 60.5373; H, 3.2873; N, 12.4583 (%); Actual: C, 58.44; H, 3.69; N, 10.77 (%).

### 2.3. Computational Methods

All calculations were carried out by using the density functional theory (DFT) approximation and utilizing the Gaussian 09 (G 09) computational codes to implement Becke's three-parameter hybrid exchange and the Lee-Yang-Parr non-local correlation functionals (B3LYP) (Santiago et al., 2022). The standard 6-311G (d,p) basis set was used for all the computations involving the lighter elements (C, H, N and O) and the LanL2DZ effective core potential for the Cu atom (Kruse et al., 2012; Adamo et al., 2013). To accurately depict the local minima connected to positive eigenvalues, every geometry will be turned to a negative vibration frequency of zero.

## 3. RESULTS AND DISCUSSION

Fig. 1 depicts the process that was used to successfully synthesize the new chemical sensor M1, M2 and M3 derivatives from the intermediate L via Duff reaction to modify the formyl group at the 8-position of the 7-Hydroxy-4-methyl coumarin, which is conveniently synthesized in an excellent yield by condensation of the resulting compound L with 1,2-diaminobenzene derivatives in an equimolar ratio to obtain imidazole group.

### 3.1. Spectroscopic Studies

$^1\text{H NMR}$  spectra further supported the bonding arrangements. All the aromatic protons appeared as a doublet at 7.75–6.88 ppm in the intermediate L, while the aromatic singlet protons showed up in the area of 6.20 ppm. The hydroxyl group was observed at 12.20 ppm. At position 10.61 ppm, a new peak appeared, clearly indicating the formation of the aldehyde group. These shifts demonstrate the intermediate L was efficiently synthesized. In sensor M1, the aromatic doublet appeared around 7.61–7.56 ppm in the region. The multiplet appeared at 7.74–7.34 ppm, indicating the benzimidazole protons. The coumarin methyl proton occurred at 2.47 ppm. Therefore, the imine band has developed due to dehydration, lending support to the synthesis of the imidazole moiety, while the  $-\text{NH}_2$  peaks have vanished. Also, in M2, the aromatic  $-\text{NH}$  group appeared at 11.09 ppm. Hence, these shifts confirm the imidazole formation. At 2.52 ppm, a singlet was observed, indicating the aromatic methyl proton. The spectral features of sensors M2 and M3 are similar but with suitable variations due to electron push-pulling groups.

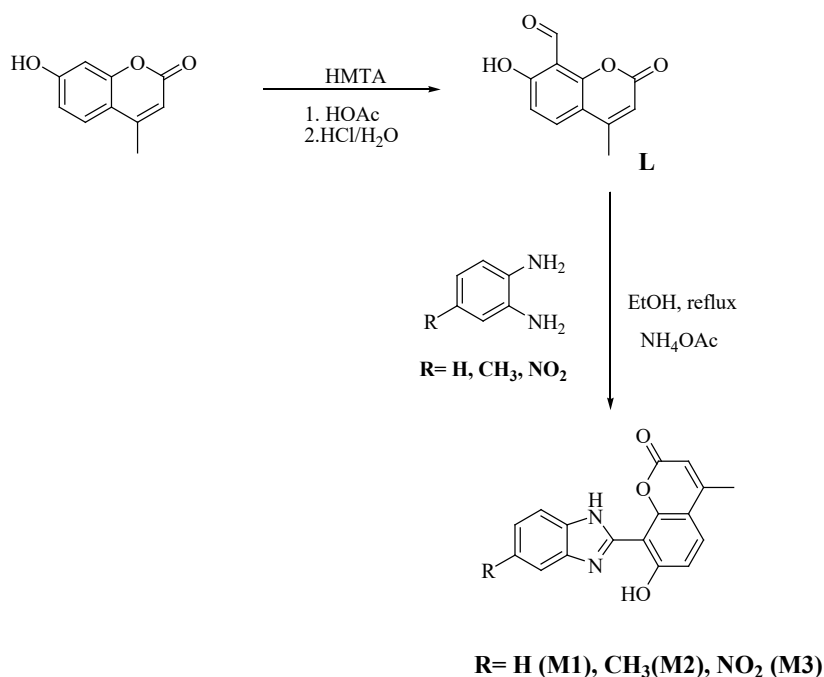


Fig. 1. Synthesis of sensors M

The chemical sensor M1, M2 and M3 mass values were observed at  $m/z = 293.21$   $[M+H]^+$  for  $C_{17}H_{12}N_2O_3$ ,  $m/z = 306.16$   $[M]^+$  for  $C_{18}H_{14}N_2O_3$ , and  $m/z = 337.09$   $[M]^+$  for  $C_{17}H_{11}N_3O_5$ , which is consistent with the theoretical values. This proves that sensor M derivatives were effectively synthesized.

### 3.2. Absorption and Emission Properties

As shown in Fig. 2, the absorption and emission spectra of sensor M derivatives, which were recorded in tetrahydrofuran (THF) solvent at ambient temperature (25 °C) in the 200–700 nm range in a  $3 \times 10^{-5}$  M concentration. The absorption bands of M derivatives were found at 315 and 330, 320 and 337, and 330 and 345 nm, attributed to the  $\pi \rightarrow \pi^*$  transition and also the electronic transition of the excited state enol tautomer ( $E \rightarrow E^*$ ). Moreover, the M2 and M3 have the redshift phenomenon; M3 introduces a robust electron-withdrawing group  $-NO_2$ , making the redshift more obvious. The UV-visible absorption spectral data are listed in Table 1.

In the photoluminescence spectra, the maximum emission was observed at 390–560 nm and the excited wavelength at 320 nm. The sensors M1 and M2 significantly change the emission intensity at 455 nm. Also, the M3 has almost no fluorescence at 455 nm, which can be attributed

to the electron-pulling effect affecting the original mechanism of electronic transition and light emission, and the fluorescence cannot be released through the emission sequence  $E \rightarrow E^* \rightarrow K^* \rightarrow K$  (Sakai et al., 2013; Honda et al., 2016).

### 3.3. Solvent Effects

The Fig. 3 depicts the solvent effect of the sensor M2. For the solvent effect, the M2 was dissolved with six different solvents THF, Toluene, dichloromethane (DCM), acetonitrile (ACN), isopropyl alcohol (IPA), methanol (MeOH)) using the  $3 \times 10^{-5}$  M concentration. In the emission spectra, the intensity was observed at 455 nm using the polar and non-polar solvents, which can be ascribed to the emission behavior via proton transfer. Simultaneously, when using the protic solvent, the emission falls at 440 nm, which corresponds to the complex caused by the solvation. Therefore, it is inferred that the solvated complex causes the emission. In addition, compared with protic solvents, low-polarity solvents have a more comprehensive range of fluorescence intensity distribution in the region of longer wavelengths. It can be inferred that protic solvents affect the intramolecular proton transfer of the compound and reduce the radioactivity in the form of proton transfer.

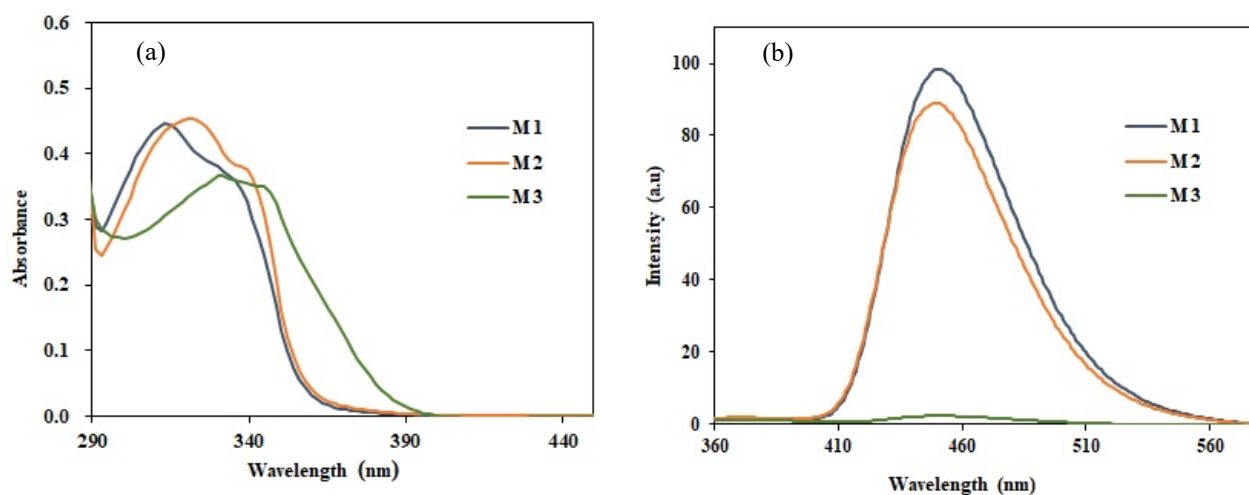


**Fig. 2.** (a) Absorption and (b) emission spectra of sensor M derivative ( $3 \times 10^{-5}$  M) in THF at room temperature ( $\lambda_{ex} = 320$  nm)

**Table 1.** UV-visible absorption, emission spectral data and determined values of the binding constant, quenching constant, detection limit and stoichiometry

Sensors	$\lambda_{abs}$ (nm) ( $\epsilon$ , 1/M cm)	$\lambda_{em}$	Binding constant ( $K_a$ , $M^{-2}$ )	Quenching Constant ( $K_{SV}$ , M)	Detection Limits (LODs)	Stoichiometry
M1	315 ( $2.22 \times 10^4$ ), 330 ( $1.91 \times 10^4$ )	455	$3.41 \times 10^9$	$1.5 \times 10^5$	$3.91 \times 10^{-9}$	2:1
M2	320 ( $2.26 \times 10^4$ ), 337 ( $1.90 \times 10^4$ )	455	$2.31 \times 10^9$	$1.0 \times 10^6$	$11.45 \times 10^{-9}$	2:1
M3	330 ( $1.82 \times 10^4$ ), 345 ( $1.75 \times 10^4$ )	455	$1.92 \times 10^9$	NA	NA	2:1

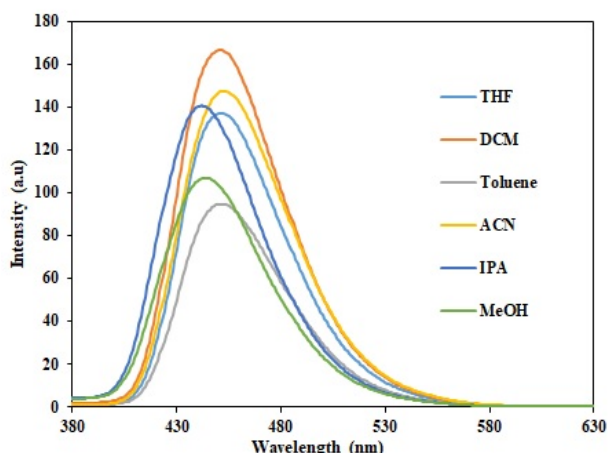


Fig. 3. Solvent effect of sensor M2 derivative ( $3 \times 10^{-5}$  M) at room temperature ( $\lambda_{ex} = 320$  nm)

### 3.4. Water Tolerance Studies

The ion recognition experiments were carried out in an aqueous solution to examine the potential application of sensor M derivatives. Based on the solvent effect, in this study we used IPA, which is more environmental friendly than ACN. Fig. 4 depicts the absorption and emission spectra sensor M2 at different H<sub>2</sub>O content in IPA solutions. In aqueous conditions, the sensor M2 was soluble in IPA at  $3 \times 10^{-5}$  M and used different H<sub>2</sub>O percentages. The M2 showed their absorption band at 310 and 330 nm; while the H<sub>2</sub>O content increased, the absorption band gradually decreased. It is speculated that the sensor's solubility has reduced due to the increase in the H<sub>2</sub>O proportion. In addition, the new absorption band at 370 nm tends to increase, which is believed to be due to the rise in H<sub>2</sub>O content, which enhances the hydrogen bond force between the solvent and the sensor, forming this absorption band. Once the H<sub>2</sub>O content reaches 90%, the appearance of the solution is in the form of a suspension. Therefore, it can be reasonably speculated that at an H<sub>2</sub>O content of 90%, the sensor aggregates, the particles become more significant, and the light transmittance decreases, making the

appearance so obvious. In the emission spectrum, while the H<sub>2</sub>O content increased, the intensity subsided, which made the change of fluorescence intensity more pronounced. The addition of H<sub>2</sub>O in the solvent system is believed to reduce the sensor's ES IPT (Excited state intramolecular proton transfer) ability. Since H<sub>2</sub>O molecules are highly polar protic solvents, they can inhibit the emission of keto form and reduce the overall emission intensity. For sensor M3, the solubility is very poor. While increase the water percentage at 70% the appearance of the solution is a suspension, due to the solubility and particle aggregation. Also, the new emission band observed at 560 nm, which can be attributed to the phenomenon of aggregation-induced emission (AIE).

### 3.5. Sensing Studies

#### 3.5.1. Selectivity of M Derivatives with Cations

The sensing behavior of probe M derivatives towards different metal ions (Li<sup>+</sup>, Cr<sup>3+</sup>, Hg<sup>2+</sup>, Cu<sup>2+</sup>, Zn<sup>2+</sup>, Cd<sup>2+</sup>, Ni<sup>2+</sup> and Pb<sup>2+</sup>) are studied using UV-Vis and emission spectroscopy. After evaluating the solubility and photochemical properties through the water content test, probes M1 and M2 were subjected to ion identification in H<sub>2</sub>O/IPA (70% water content). Adding the metal ions caused noticeable changes in the absorption and emission spectra. Fig. 5 shows the sensor M1 selectivity of different metal ions added. When 70% water content was added to the probes M1 and M2, the absorption bands were found at 310, 315 and, 330, 337 nm. When the addition of metal ions to probes M1 and M2, a specific change was observed, and the absorption also shifted. While adding 3.0 equivalents of different metal ions to the probe, a distinct difference was observed only in the Cu<sup>2+</sup> and Hg<sup>2+</sup> ions, and the absorption bands at 310 and 330 nm have been decreased; a new absorption band at 360 nm has been enhanced. There is no significant change that occurred after the addition of Li<sup>+</sup>, Cr<sup>3+</sup>, Cd<sup>2+</sup>, Ni<sup>2+</sup> and Pb<sup>2+</sup> metal ions. In identifying Cu<sup>2+</sup> ions, the absorption spectrum showed a downward trend.

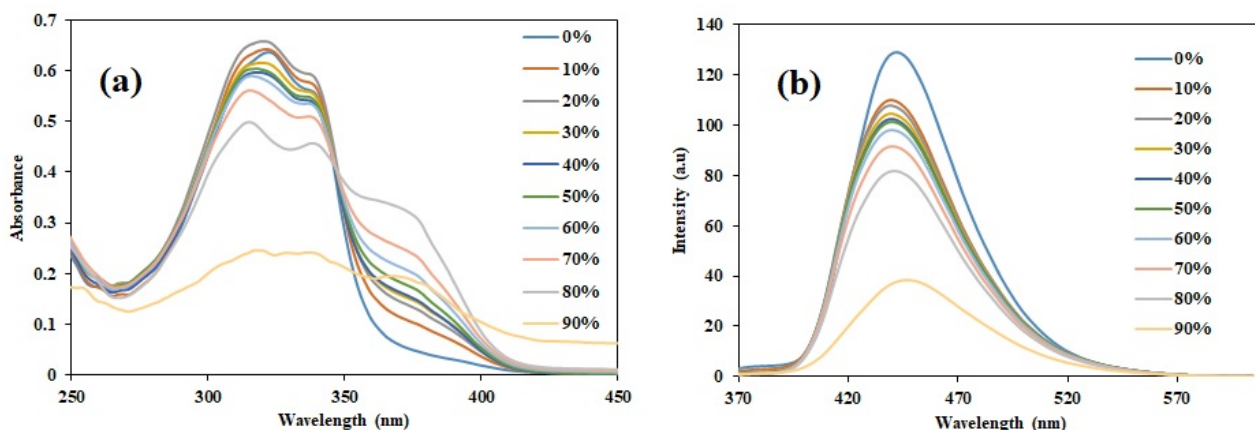
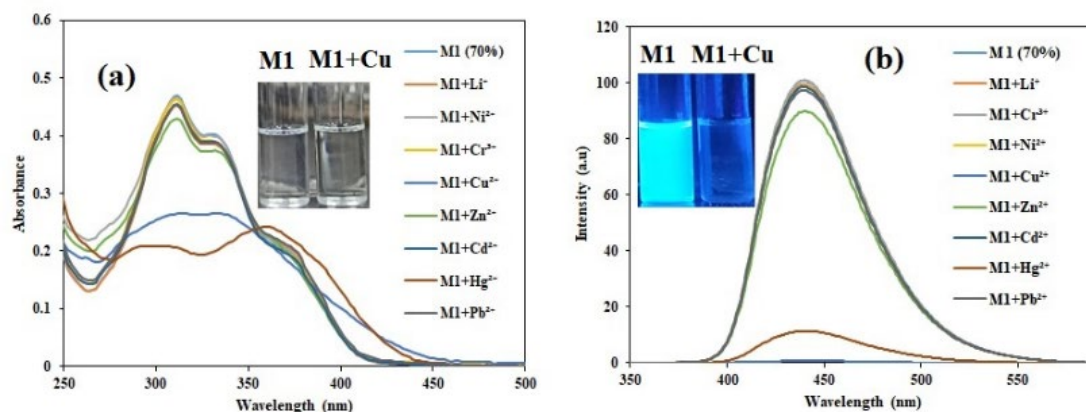


Fig. 4. (a) UV-Vis absorption and (b) Fluorescence spectra of sensor M2 ( $3 \times 10^{-5}$  M) in IPA with different H<sub>2</sub>O ratios ( $\lambda_{ex} = 320$  nm)



**Fig. 5.** (a) UV-Vis and (b) Emission spectral changes of sensor M1 (30  $\mu\text{M}$ ) upon the addition of different cations in  $\text{H}_2\text{O}/\text{IPA}$  (v/v = 7:3,  $\lambda_{\text{exc}}$  = 320 nm)

In the emission spectra, the intensity of the probe M1 and M2 showed slight shifts in the presence of  $\text{Li}^+$ ,  $\text{Cr}^{3+}$ ,  $\text{Cd}^{2+}$ ,  $\text{Ni}^{2+}$  and  $\text{Pb}^{2+}$ . However,  $\text{Hg}^{2+}$  ions exhibited extremely noticeable quenching. In the presence of  $\text{Cu}^{2+}$  ions, a highly selective “turn-off” fluorescence has been observed in the probe M1. It quenches the fluorescence entirely in the presence of  $\text{Cu}^{2+}$  ions. In the case of probe M2, the  $\text{Cu}^{2+}$  ion showed very distinct quenching activity due to the influence of the electron-donating group. In recognition of  $\text{Cu}^{2+}$ , the effect of fluorescence emission is less significant than that of probe M1, and also, the complex emission wavelength is slightly redshifted at 455 nm. However, the  $\text{Hg}^{2+}$  ion exhibited much more quenching action than any other metal ions tested, completely suppressing both probes M1 and M2 fluorescence. These emission results are consistent with the absorption spectrum. The obtained quenching of the fluorescence might be the formation of M and  $\text{Cu}^{2+}$  ions, facilitating excited-state energy transfer or charge transfer (Kwon et al., 2011). A possible mechanism for the high selectivity of M can be due to the paramagnetic nature and unoccupied 3d orbital of  $\text{Cu}^{2+}$  ions (Kwon et al., 2011). Therefore, the probes formed a stable complex with  $\text{Cu}^{2+}$  ions (Kwon et al., 2011). Hence, these findings confirmed that the probe M derivative could be used as a selective fluorescent chemosensor for  $\text{Cu}^{2+}$  detection. The fluorescence quantum yields significantly reduced from 0.180 to 0.039 for sensor M2 and its  $\text{Cu}^{2+}$  complex when measured at room temperature with anthracene ( $\Phi_{\text{F}} = 0.36$  in ethanol) as the standard (Williams et al., 1983). Moreover, the sensor M derivatives and  $\text{Cu}^{2+}$  ions were detected by under UV light. Upon the addition of  $\text{Cu}^{2+}$  ions, the fluorescence does not exist. In the presence of  $\text{Cu}^{2+}$  ions, a highly selective “turn-off” fluorescence has been appeared.

### 3.5.2. Titration of Sensor M1 with $\text{Cu}^{2+}$

Fig. 6 depicts the titration study of probe M1 and the spectral changes upon titrating a fixed concentration ( $3 \times 10^{-5}$  M) against 0.1 ~ 2.0 equivalent of  $\text{Cu}^{2+}$  ( $10^{-4}$  M) in  $\text{IPA}:\text{Water} = 3:7$  (v/v) at 25°C were used.

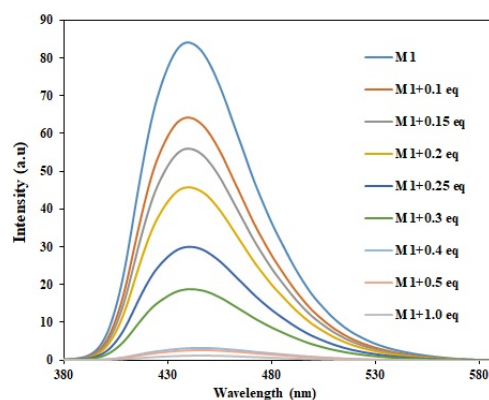


**Fig. 6.** Fluorescence spectra of sensor M1 with different equivalent of  $\text{Cu}^{2+}$  ions in  $\text{H}_2\text{O}/\text{IPA}$  (7:3)

In the emission spectrum, while adding  $\text{Cu}^{2+}$  ions to probe M1, the emission intensity gradually decreased at 440 nm. Likewise, adding 1.0 equivalent of  $\text{Cu}^{2+}$  ions to M1, the emission reaches the minimum value and is completely quenched. When increasing the  $\text{Cu}^{2+}$  content, almost there is no shift observed in the emission spectrum. A change was observed after adding 0.1 equivalent of (1.0  $\mu\text{M}$ ) of metal ions, indicating that sensor M1 has high sensitivity. The sensors M2 and M3 have similar characteristics.

### 3.6. Binding Mode

Sensor M1 binding stoichiometry was analyzed using Job's plot, obtained from the emission spectra, denoting the maximum emission intensity. The sensor M1 molar fraction was found at 0.66 (Fig. 7a), indicating that it formed with  $\text{Cu}^{2+}$  complex in 2:1 binding stoichiometry. As a result, the emission spectrum agreed with these findings.

In practical applications, reversibility is an essential factor for evaluating chemosensors. The ethylenediaminetetraacetic acid (EDTA) was used as a reversing agent with the addition of 1 eq. EDTA to the sensor M1 solution, the emission intensity of the receptor M1 with  $\text{Cu}^{2+}$  complex returned to its original stage,

presumably due to the removal of copper ions from the M1-Cu<sup>2+</sup> complex. When an equal amount of Cu<sup>2+</sup> was added to the solution, the quenched fluorescence almost returned up to 80% to its M1-Cu<sup>2+</sup> level of intensity. These findings show that sensor M derivatives can be used as a reversible sensor with high sensitivity and selectivity for detecting Cu<sup>2+</sup> ions in an aqueous medium (Fig. 7b).

Moreover, the mass spectra provided further confirmation of this binding process (Fig. 8). The ESI-MS of the [M2-Cu]<sup>+</sup> complex shows the peak at 675.3, which corresponds closely to the calculated mass of [M2-Cu]<sup>+</sup>, which is 675.18 (2:1). Thus, we conclude that Cu<sup>2+</sup> coordinated with the probe M2.

The plot linearity also further supports the stoichiometry ratio. The binding constant of the sensor M1 with Cu<sup>2+</sup> is calculated from the Benesi-Hildebrand plot (Fig. 9a). From the ratiometric fluorescence titration data, the binding constant is calculated using  $\alpha^2(1-\alpha)$  versus  $1/[Cu^{2+}]$ , which

is found to be  $K_a 3.41 \times 10^9 / M^2$ . The limit of detection (LOD) is a crucial aspect of ion sensing, which is necessary to detect the probes at low concentrations for numerous practical uses. Fig. 9b depicts the detection limit of sensor M1-Cu<sup>2+</sup>. The LOD of Cu<sup>2+</sup> using M1 and M2 is calculated from the calibration curve of ratiometric fluorescence titration. According to the IUPAC method, the LOD is calculated using  $3sB/m$ , where  $sB$  is the standard deviation of the blank solution, and  $m$  is the slope of the calibration curve. The result shows that using M1 and M2 of Cu(II) shows  $3.912 \times 10^{-9}$  and  $11.448 \times 10^{-9}$  M. The calculated LOD value is much lower than the allowed limit ( $\sim 20$  nM) in drinking water set by WHO (Saleem et al., 2018; Liu et al., 2019). Table 2 demonstrates that sensor M derivative could be used as a fluorescence chemosensor with high selectivity and sensitivity for Cu<sup>2+</sup> was comparable with those reported sensors in recent years (Zhang et al., 2013; Wang et al., 2014; Wang et al., 2015; Shi et al., 2022).

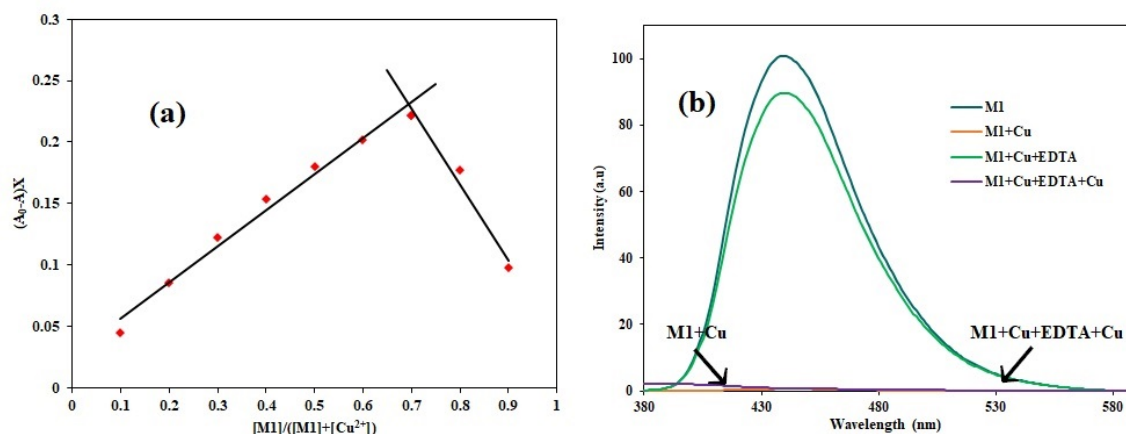


**Fig. 7.** (a) Job's plot for sensor M1-Cu<sup>2+</sup> formation in a 2:1 binding ratio (b) Fluorescence spectra reversibility of sensor M1-Cu<sup>2+</sup> with the addition of EDTA

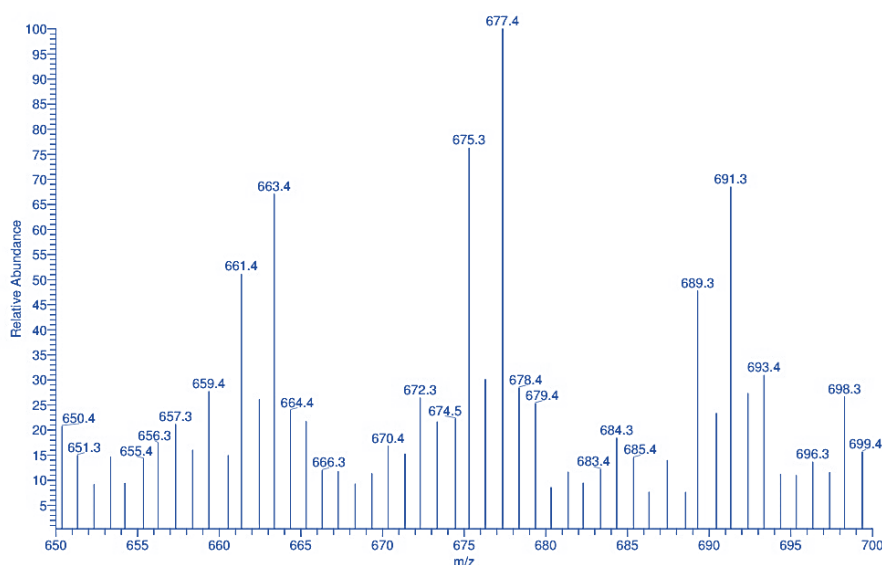


**Fig. 8.** ESI-MS spectra of sensor M2-Cu<sup>2+</sup> complex

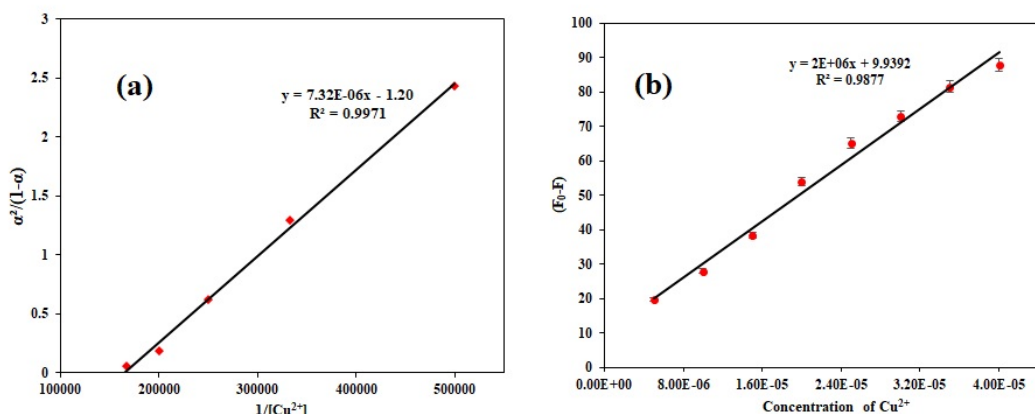


**Fig. 9.** (a) The Benesi-Hildebrand plot shows the linear relationship between sensor M1 and  $\text{Cu}^{2+}$  complex. (b) The calibration plot of sensor M1- $\text{Cu}^{2+}$

**Table 2.** Comparison of sensing performance of sensor M derivatives with reported chemosensors for fluorescent detection of  $\text{Cu}^{2+}$  ions

Method	Detection limit (M)	Advantages	Disadvantages	Reference
Fluorescent rhodamine-based chemosensors Iridium(III) complex	$4.5 \times 10^{-9}$	Selective towards $\text{Cu(II)}$ ions	It needs organic solvent for detection	Wang et al. (2014)
Colorimetric pyrazine-based chemosensor	$2.47 \times 10^{-8}$	Selective towards $\text{Cu(II)}$ ions	Low sensitivity	Shi et al. (2020)
Fluorescent anthracene and pyridine-based chemosensor	$8.63 \times 10^{-8}$	Selective towards $\text{Cu(II)}$ ions	It needs organic solvent for detection	Wang et al. (2015)
Fluorescent rhodamine-based chemosensor	$8.00 \times 10^{-7}$	Selective towards $\text{Cu(II)}$ ions	It needs organic solvent for detection	Zhang et al. (2013)
Fluorescent indole-based chemosensor K2	$8.42 \times 10^{-10}$	Selective towards $\text{Cu(II)}$ ions	It needs organic solvent for detection	Kumarasamy et al. (2022)
Fluorescent Pyridine-based benzimidazole chemosensor	$3.24 \times 10^{-9}$	Selective towards $\text{Cu(II)}$ ions	It needs organic solvent for detection	Kumarasamy et al. (2023)
Fluorescent Benzimidazole-based coumarin chemosensor M1	$3.91 \times 10^{-9}$	Selective towards $\text{Cu(II)}$ ions	It needs organic solvent for detection	This study
Fluorescent Benzimidazole-based coumarin chemosensor M2	$11.45 \times 10^{-9}$	Selective towards $\text{Cu(II)}$ ions	It needs organic solvent for detection	This study

The Stern Volmer constant is calculated using  $F_0/F_i$  versus the concentration of the quencher, which is evaluated from the ratiometric fluorescence titration data. The Stern Volmer constant of sensors M1 and M2 was  $K_{sv}=1.5 \times 10^5$  and  $K_{sv}=1.0 \times 10^6$  M.

### 3.7 Analysis of $\text{Cu(II)}$ in Water Samples

In order to study the real sample analysis of sensor M2, two different types of recovery experiments were performed using  $\text{Cu}^{2+}$  metal ions. The water samples used in these studies included tap water and distilled water. The recovery of the water sample analysis is summarized in Table 3. Real samples are examined in triplicate analysis, which shows good relative standard deviation (RSD) with acceptable recovery. The recovery percentage is greater than 98%, which shows that the proposed sensor M2 can be used for the  $\text{Cu}^{2+}$  analysis in real samples. The outcome of this investigation determines the potential of the sensor.

### 3.8. Theoretical Calculations

The binding mechanism between the sensor M derivatives and their complexes  $\text{M-Cu}^{2+}$  was further confirmed by theoretical calculations at BLYP/6311G\*\* basic set using Gaussian 09 software package, which is used to determine the various quantum chemical properties, molecular energy, ESP charges, frontier molecular orbital and among others. The photophysical characteristics and hydrogen bonding interactions of molecules are greatly aided by the electrostatic potential, which was constructed on a surface with unchanging electron density. Free ligand sensor M derivatives molecular electrostatic potential is shown in a three-dimensional representation in Fig. 10. Bright red denotes the most significant negative region favored for the electrophilic site. Moreover, blue represents the most critical positive zone, the preferred place for nucleophilic sites. The  $\text{Cu}^{2+}$  complex shows dentate coordination of imidazolyl N and coumarin O groups, whereas the free ligand displays substantially pre-organized



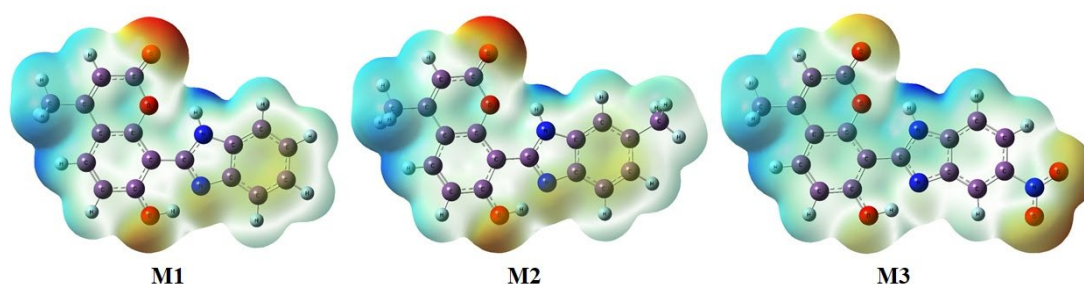
planar geometry. The results further demonstrate that sensor M derivatives have dentate coordination with the complex tetrahedral geometry.

The Fig. 11 shows the optimized M and M-Cu<sup>2+</sup> structures. Table 4 compiles the results of the calculations for the HOMO and LUMO energy gap values for M and M-Cu<sup>2+</sup>. The HOMO and LUMO levels were filled in sensor M derivatives, while the LUMO of sensors M1 and M2 were mainly located in the coumarin ring. In the case of sensor M3, the LUMO is presented primarily in the benzimidazole ring due to its electron-withdrawing nature. When the free

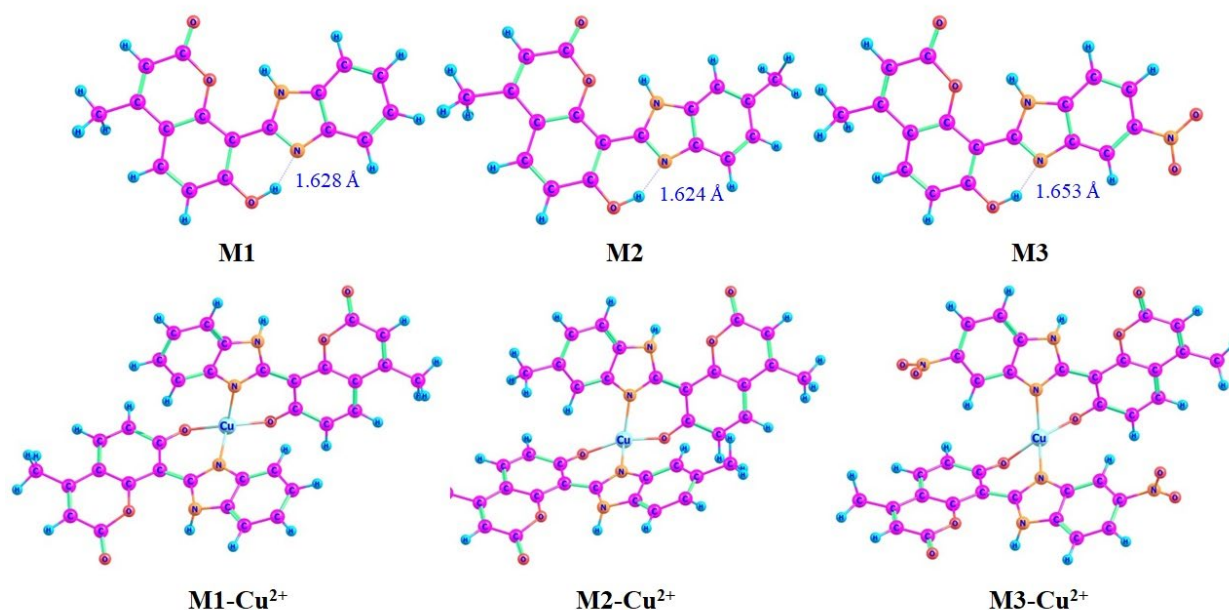
sensor M interacts with Cu<sup>2+</sup>, the corresponding energy levels of HOMO and LUMO were distributed entirely throughout the molecules, except the benzimidazole phenyl ring (Fig. 12). The selected bond length is listed in Table 5. In addition, the interaction energies of sensors M with their Cu<sup>2+</sup> complexes were computed using ideal energies ( $E_{\text{interaction}} = E_{\text{product}} - E_{\text{reactants}}$ ) and were found to be -211.548, -185.957, -174.191 kcal/mol. The results show the interaction energy of copper complex in the order of M3-Cu<sup>2+</sup> > M2-Cu<sup>2+</sup> > M1-Cu<sup>2+</sup>, which is following the binding constant trend.

**Table 3.** Analysis of Cu(II) in different water using proposed sensor M2

Real sample	Cu(II) contents (μM)		Recovery (%)	RSD (%) (n = 3)
	Spiked	Found		
Distilled water	5	4.97	99.44	1.45
	10	9.99	99.92	1.33
Tap water	5	4.92	98.52	2.01
	10	9.81	98.13	1.35



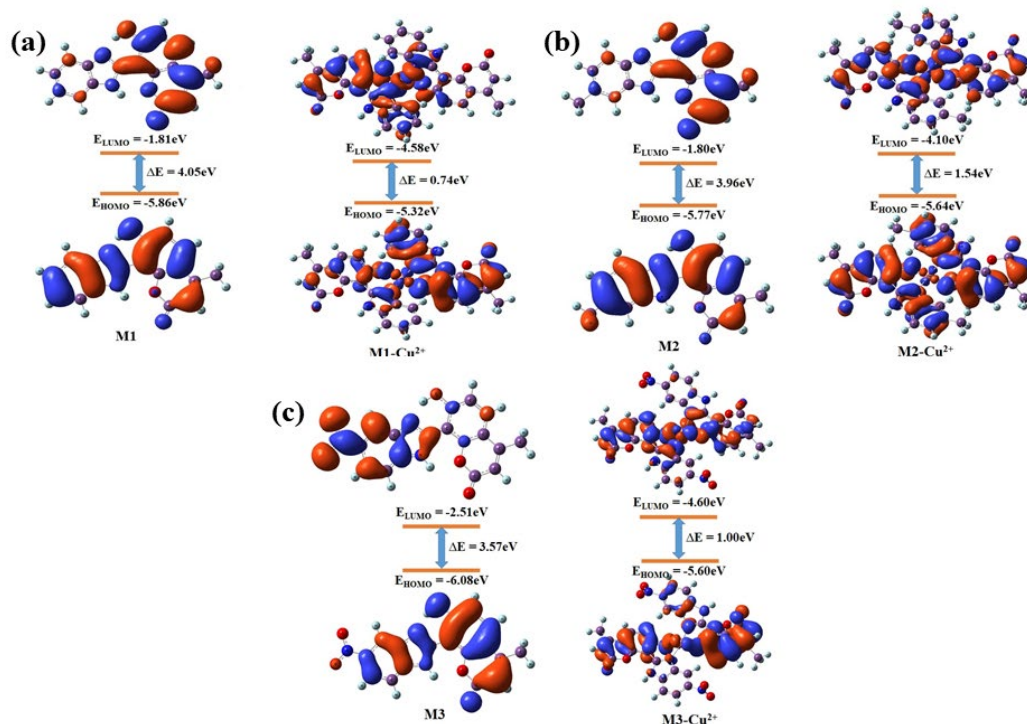
**Fig. 10.** Molecular electrostatic potential is mapped on the surface of the optimized molecular geometry of sensor M using the DFT/B3LYP method



**Fig. 11.** Optimized molecular geometry of sensor M1, M2 and M3 with Cu<sup>2+</sup> ion using the DFT/B3LYP method

**Table 4.** Experimental prediction of quantum chemical parameters for sensor M derivative and their complexes

S. No	System	Energy (Kcal/mol)	DM (Debye)	HOMO (eV)	LUMO (eV)	Energy Gap (eV)
1	M1	-623804.60	3.77	-5.86	-1.81	-4.05
2	M2	-648578.51	3.21	-5.77	-1.80	-3.96
3	M3	-752654.28	10.94	-6.08	-2.51	-3.57
4	M1-Cu	-1370834.35	3.63	-5.32	-4.58	-0.74
5	M2-Cu	-1420419.75	0.47	-5.64	-4.10	-1.54
6	M3-Cu	-1299395.02	22.44	-5.60	-4.60	-1.00


**Fig. 12.** The frontier molecular orbitals of sensor M1, M2 and M3 with  $\text{Cu}^{2+}$  ion, by using the DFT/B3LYP method

In addition, the energy gap values between the M and  $\text{M-Cu}^{2+}$  complex were calculated. The HOMO and LUMO energy gap of sensor M and its complexes  $\text{M-Cu}^{2+}$  were found to be 4.05, 3.96, 3.57 eV and 0.74, 1.54, 1.00 eV, respectively. As a result, the coordination between the sensor M and their complexes  $\text{M-Cu}^{2+}$  lowered the HOMO and LUMO energy levels and stabilized the sensing molecule  $\text{M-Cu}^{2+}$ . The intramolecular charge transfer interaction between the imidazolyl and coumarin molecules is shown by a redistribution of electron density during the HOMO-LUMO transition after forming the  $\text{M-Cu}^{2+}$  complex. These stimulated results agreed with those of the tests.

**Table 5.** The selected bond length of the  $\text{M-Cu}^{2+}$  tetrahedral complex

Complex	$\text{O}_1\text{---Cu}$	$\text{N}_1\text{---Cu}$	$\text{O}_2\text{---Cu}$	$\text{N}_2\text{---Co}$
M1-Cu	1.960	1.938	1.957	1.936
M2-Cu	1.981	1.964	1.963	2.007
M3-Cu	2.031	2.052	2.078	2.004

## 4. CONCLUSION

A benzimidazole-based coumarin-derived fluorescent chemosensor with high sensitivity and selectivity towards  $\text{Cu}^{2+}$  has been developed.  $\text{Cu}^{2+}$  ions significantly quenched the fluorescence emission, while other metal cations had no interference. The detection limit of probe M1 has been found to be  $\text{Cu}^{2+}$  for 3.9 nM. The Job's plot studies indicate that M1 binds with a  $\text{Cu}^{2+}$  2:1 ratio. The reversibility of M1 sensing of  $\text{Cu}^{2+}$  is demonstrated by the recovery of fluorescence intensity with  $\text{Na}_2\text{EDTA}$ . DFT calculations suggest that intramolecular charge transfer is the cause of the fluorescence quenching process in  $\text{M1-Cu}^{2+}$ . In future studies, we will investigate the biological and environmental application of the  $\text{Cu}^{2+}$  Chemosensor based on benzimidazole-based coumarin moiety.

## ACKNOWLEDGMENTS

We are thankful to the Chaoyang University of

Technology, Taiwan, for providing the project funding and instrumental facilities for our research group. The authors thank the Instrument Center of National Chung Hsing University, Taiwan, for elementary analysis and LC-MS/MS.

## REFERENCES

- Adamo, C., Jacquemin, D. 2013. The calculations of excited-state properties with time-dependent density functional theory. *Chemical Society Reviews*, 42, 845–856.
- Devendhiran, T., Kumarasamy, K., Lin, M.C., Yang, Y.X. 2021. Synthesis and physical studies of coumarin-based chemosensor for cyanide ions. *Inorganic Chemistry Communications*, 134, 108951–108960.
- Duan, Y-W., Tang, H-Y., Guo, Y., Song, Z-K., Peng, M.J., Yan, Y. 2014. The synthesis and study of the fluorescent probe for sensing  $\text{Cu}^{2+}$  based on a novel coumarin Schiff-base. *Chinese Chemical Letters*, 25, 1080–1086.
- Feng, Y., Yang, Y., Wang, Y., Qiu, F., Song, X., Tang, X., Zhang, G., Liu, W. 2019. Dual-functional colorimetric fluorescent probe for sequential  $\text{Cu}^{2+}$  and  $\text{S}^{2-}$  detection in biomaging. *Sensors and Actuators B: Chemical*, 288, 27–37.
- Gunnlaugsson, T., Glynn, M., Tocci, G.M., Kruger, P.E., Pfeffer, F.M. 2006. Anion recognition and sensing in organic and aqueous media using luminescent and colorimetric sensors. *Coordination Chemistry Reviews*, 250, 3094–3117.
- Haugland, R.P. 2002. *Handbook of fluorescent Probes and Research Products*, 9<sup>th</sup> ed.; Molecular Probe, Eugene.
- Honda, T., Ishida, Y., Arai, T. 2016. Effect of intramolecular hydrogen bonding on photocleavage reaction of (3-Benzazolyl-2-hydroxy-5-methylphenyl) methyl acetate. *Bulletin of the Chemical Society of Japan*, 89, 1321–1327.
- Huang, P.J., Kumarasamy, K., Devendhiran, T., Chen, Y.C., Dong, T.Y., Lin, M.C. 2021. BODIPY-based hydroxypyridyl derivative as a highly  $\text{Ni}^{2+}$ -selective fluorescent chemosensor. *Journal of Molecular Structure*, 1246, 131281–131289.
- Jung, H.S., Kwon, P.S., Lee, J.W., Kim, J.I., Hong, C.S., Kim, J.W., Yan, S., Lee, J.Y., Lee, J.H., Joo, T., Kim, J.S. 2009. Coumarin-derived  $\text{Cu}^{2+}$ -selective fluorescence sensor: Synthesis, mechanisms, and applications in living cells. *Journal of the American Chemical Society*, 139, 2008–2012.
- Kim, H.N., Lee, M.H., Kim, H. J., Kim, J.S., Yoon, J. 2008. A new trend in rhodamine-based chemosensors: Application of spirolactam ring-opening to sensing ions. *Chemical Society Reviews*, 37, 1465–1472.
- Kim, S.H., Kim, J.S., Park, S.M., Chang, S.K. 2006.  $\text{Hg}^{2+}$ -selective OFF-ON and  $\text{Cu}^{2+}$ -selective ON-OFF type fluorophore based upon cyclam. *Organic Letters*, 8, 371–374.
- Kruse, H., Georigk, L., Grimme, S. 2012. Why the standard B3LYP/6-31G\* model chemistry should not be used in DFT calculations of molecular thermochemistry: Understanding and correcting the problem. *Journal of Organic Chemistry*, 77, 10824–10834.
- Kumarasamy, K., Devendhiran, T., Lin, M.C., Chien, W.J., Ramasamy, S.K., Manickam, S., Yang, J. 2022. Synthesis and recognition behaviour studies of indole derivatives. *Inorganic Chemistry Communications*, 145, 110020–110032.
- Kumarasamy, K., Devendhiran, T., Chien, W.J., Lin, M.C., Ramasamy, S.K., Liao, Y. 2023. Synthesis and recognition behaviour studies of benzimidazole derivative containing pyridine moiety. *Journal of Photochemistry and Photobiology A: Chemistry*, 445, 115067–115076.
- Kwon, J.E., Park, S.Y. 2011. Advanced organic optoelectronic materials: Harnessing excited-state intramolecular proton transfer (ESIPT) process. *Advanced Materials* 23, 3615–3642.
- Liu, H., Cui, S., Shi, F., Pu, S. 2019. A diarylethylene based multi-functional sensor for fluorescent detection of  $\text{Cd}^{2+}$  and colorimetric detection of  $\text{Cu}^{2+}$ . *Dyes and Pigments*, 161, 34–43.
- Mercer, J.F.B. 2001. The molecular basis of copper-transport diseases. *Trends in Molecular Medicine*, 7, 64–73.
- Puig, S., Thiele, D.J. 2002. Molecular mechanisms of copper uptake and distribution. *Current Opinion in Chemical Biology*, 6, 171–180.
- Rae, T.D., Schmidt, P.J., Pufahl, R.A., Culotta, V.C., O'Halloran, T.V. 1999. Undetectable intracellular free copper: the requirement of a copper chaperone for superoxide dismutase. *Science*, 284, 805–808.
- Sahoo, S.K., Sharma, D., Moirangthem, A., Kuba, A., Thomas, R., Kumar, R., Kuwar, A., Choi, H-J., Basu, A. 2016. Pyridoxal derived chemosensor for chromogenic sensing of  $\text{Cu}^{2+}$  and fluorogenic sensing of  $\text{Fe}^{3+}$  in semi-aqueous medium. *Journal of Luminescence*, 172, 297–303.
- Sakai, K., Ishikawa, T., Akutagawa, T. 2013. A blue-white-yellow-tunable excited state intramolecular proton transfer (ESIPT) fluorophore: Sensitivity to polar-nonpolar solvent ratios. *Journal of Material Chemistry*, 1, 7866–7871.
- Saleem, M., Rafiq, M., Hanif, M., Shaheen, M.A., Seo, S-Y. 2018. A brief review on fluorescent copper sensor based on conjugated organic dyes. *Journal of Fluorescence*, 28, 97–95.
- Santiago, P.H.O., Duarte, E.A., Nascimento, É.C.M., Martins, J.B.L., Castro, M.S., Gatto, C.C. 2022. A binuclear copper(ii) complex based on hydrazone ligand: characterization, molecular docking, and theoretical and antimicrobial investigation. *Applied Organometallic Chemistry*, 36, 1–16.
- Sathiyam, G., Balasubramaniam, B., Ranjan, S., Chatterjee, S., Sen, P., Garg, A., Gupta, R., Singh, A. 2019. A novel star-shaped triazine-tripheylamine-based fluorescent chemosensor for the selective detection of picric acid. *Materials Today Chemistry*, 12, 178–186.

- Sathiyar, G., Chatterjee, S., Sen, P., Garg, A., Gupta, R., Singh, A. 2019. Thiazolothiazole-based fluorescence probe towards detection of copper and iron ions through formation of radical cations. *ChemistrySelect*, 4, 11718–11725.
- Sathiyar, G., Mathivanan, D., Bhuvaneshwari, B., Garg, A., Gupta, R.K., Singh, A. 2021. Olefin-linked conjugated fluorescent oligomer: Design, synthesis, photophysical studies and detection of nitroaromatic compounds (NACs) in aqueous media. *Sensors and Actuators A: Physical*, 331, 113026.
- Sathiyar, G., Skathivel, P. 2016. A multibranch carbazole linked triazine based fluorescent molecule for the selective detection of picric acid. *RSC Advances*, 6, 106705–106715.
- Sathiyar, G., Thangamuthu, R., Sakthivel, P. 2016. Synthesis of carbazole-based copolymers containing carbazole-thiazolo [5,4-d] thiazole groups with different dopants and their fluorescence and electrical conductivity applications. *RSC Advances*, 6, 63196–69205.
- Strausak, D., Mercer, J.F.B., Dieter, H.H., Stremmel, W., Multhaup, G. 2001. Copper in disorders with neurological symptoms: Alzheimer's, Menkes, and Wilson diseases. *Brain Research Bulletin*, 55, 175–185.
- Valentine, J.S., Hart, P.J. 2003. Misfolded CuZnSOD and amyotrophic lateral sclerosis. *Proceedings of the National Academy of Sciences*, 100, 3617–3622.
- Venkatesan, V., Selva Kumar, R., Ashok Kumar, S.K., Sahoo, S.K. 2019. Dual optical properties of new Schiff base based on bithiophene for sensing of Cu<sup>2+</sup> in protic media. *Journal of Molecular Structure*, 1198, 126906–126914.
- Waggoner, D.J., Bartnikas, T.B., Gitlin, J.D. 1999. The role of copper in neurodegenerative disease. *Neurobiology of Disease*, 6, 221–230.
- Williams, A.T.R., Winfield, S.A., Miller, J.N. 1983. Relative fluorescence quantum yields using a computer-controlled luminescence spectrometer. *Analyst*, 108, 1067–1071.
- Yu, M., Shi, M., Chen, Z., Li, X., Gao, Y., Xu, J., Yang, H., Zhou, Z., Yi, T., Huang, C. 2008. Highly sensitive and fast responsive fluorescence turn-on chemodosimeter for Cu<sup>2+</sup> and its application in live cell imaging. *Chem*, 14, 6892–6900.
- Yuan, L., Lin, W., Yang, Y., Song, J., Wang, J. 2011. Rational design of a highly reactive ratiometric fluorescent probe for cyanide. *Organic Letters*, 13, 3730–3733.